Journal of Mathematical Sciences
https://doi.org/10.1007/s10958-026-08266-w

NON-UNIQUE SOLUTION WITH DISCONTINUOUS VELOCITY FOR COLLISION OF ELASTIC BAR WITH HIGH INITIAL SPEED BY ST-PDAS RESTORING ENERGY

Victor A. Kovtunenko[1,2]

Received: 1 December 2025 / Revised: 15 February 2026 / Accepted: 25 February 2026
© The Author(s) 2026

Abstract
Motivated by inequality constraints appearing in optimization context, we study non-smooth variational problems and methods appropriate for their accurate solution. The use of Lagrange multipliers and merit functions leads to semi-smooth Newton methods and equivalent primal-dual active-set iterative algorithms. For application in dynamic contact mechanics, we investigate the collision of a rigid obstacle by a one-dimensional elastic bar. The problem is described by the wave equation subjected to complementarity conditions, which weak solution is characterized by a discontinuous velocity. The collision problem may have a non-unique solution for a high initial speed exceeding the propagation speed of elastic waves. Multiple solutions are constructed analytically. For the unique solution that restores the energy of the bar after rebound, the primal-dual active-set method is implemented within space-time finite elements.

Keywords Impact contact dynamics · Variational inequality · Discontinuous velocity · Space-time finite element · Primal-dual active set

Introduction

The theory of dynamic contact problems and their solution belongs to the field of computational and impact mechanics, see [1, 2]. Based on the method of singular integral equations [3], some of two- and three-dimensional dynamic and crack problems of the linear elasticity over unbounded domains were reduced to singular integral equations [4–6]. The variational theory of contact problems stated in non-smooth bounded domains was developed in the monograph [7] and continued further [8–11]. For the related modeling of viscous bodies, we refer the reader to [12–14]. Using the viscosity approach, solvability of dynamic variational inequalities can be found, e.g., in [15, 16]. We cite [17, 18] for proper numerical methods and computer-based simulation techniques, to [19–22] for advanced optimization, and to [23–26] for other nonlinear issues related to the theory of dynamic and constrained models.

The basics of finite element approximation used in the field can be found in [27]. For a time-stepping, implicit numerical schemes of θ-type, Newmark-β, and Hilber–Hughes–Taylor (HHT)-α families were developed. There are used Taylor series approximating acceleration that assumes a continuous velocity. To solve effectively contact problems and the corresponding variational inequalities, a semi-smooth Newton (SSN) concept was developed [28]. The Newton-type methods obey a locally super-linear convergence rate and can be implemented in the form of a primal-dual active set (PDAS) algorithm. Its property of global, moreover, monotone convergence is provided by the M-matrix condition. For a variety of static problems in mechanics, the complete numerical analysis of SSN-based algorithms was carried out rigorously, see, e.g., [29, 30]. Within the theory of

✉ Victor A. Kovtunenko
victor.kovtunenko@uni-graz.at

[1] Department of Mathematics and Scientific Computing, University of Graz, NAWI Graz, Heinrichstr.36, Graz 8010, Austria

[2] Lavrent'ev Institute of Hydrodynamics, Siberian Division of the Russian Academy of Sciences, Novosibirsk 630090, Russia

Published online: 06 March 2026

dynamic contact problems, numerical simulations with the help of PDAS approach are referred to in [31, 32]. Incorporating the PDAS concept into HHT-α time-stepping schemes was suggested and implemented in [33, 34].

In the paper, we study a linear elastic bar which starts moving with an initial speed and then collides with a stationary rigid obstacle. The collision benchmark for an initially undeformed bar dropped against a ground with an initial speed stems from [35, 36]. The other benchmark from [37–39] suggests the ground impacted by an initially deformed bar without initial speed. In both cases, two bodies have different velocities; hence, elastic response during the impact may produce instabilities. The properties of dynamic stability are crucial for constructing a numerical solution. For this task, finding an exact solution of the problem is very much helpful. To treat discontinuous velocities numerically, space-time (ST) methods are well suited, see [40, 41]. We have incorporated the PDAS concept within a full ST-discretization in [42, 43].

In the latter work [43], the collision with a discontinuous velocity was studied for moderate initial speeds less than the propagation speed of elastic waves. This provides a unique solution to the problem, which can be constructed along the characteristics in 2D, where the first dimension is time and the second dimension is space. The present contribution deals with non-unique solutions of the collision problem as a consequence of high initial speeds exceeding the threshold. The novelty consists in construction of multiple analytical solutions to the wave equation, expressed by piecewise-linear functions over rectangle domains. Further developments of the ST-PDAS algorithm yield a highly precise numerical solution for the collision benchmark attained in only few iterates.

For illustration, let us consider a unit point mass located at the deep $x = -H < 0$. The mass starts motion with an initial speed $v_0 > 0$ without damping until it collides with the obstacle $x = 0$ at the time $\tau = H/v_0$. Its trajectory $x = u(t)$ with respect to the origin can be described in time $t > 0$ by the equation of motion, which is supported by initial conditions, and contact conditions expressed in the complementarity form:

$$\begin{cases} u_{,tt}(t) = \lambda(t), \quad 0 \geq u(t) \perp \lambda(t) \leq 0 \quad \text{for } t > 0, \\ u(0) = -H, \quad u_{,t}(0) = v_0. \end{cases} \tag{1.1}$$

Here the first time derivative $u_{,t} = \partial u/\partial t$ implies velocity, and the second time derivative $u_{,tt} = \partial^2 u/\partial t^2$ yields acceleration. The inequality $u \leq 0$ guarantees non-penetration through the obstacle, and the dual variable λ implies a contact force that should be non-tensile. The system (1.1) possesses multiple solutions:

$$\begin{cases} u(t) = v_0(t-\tau), & \lambda(t) = 0 \quad \text{for } t \in (0, \tau) \\ u(t) = 0, & \lambda(t) = 0 \quad \text{for } t \in (\tau, t_1) \\ u(t) = v_1(t_1 - t), & \lambda(t) = 0 \quad \text{for } t > t_1 \end{cases} \tag{1.2}$$

with an arbitrary time $t_1 \geq \tau$ and a velocity $v_1 \geq 0$ of rebound, see Fig. 1. Here, $\lambda(t) = 0$ during the second stage corresponds to a grazing contact. The rebound is commonly quantified with the help of the restitution coefficient:

$$e := \frac{v_1}{v_0} \begin{cases} = 0 & \text{for perfectly inelastic collision} \\ \in (0, 1) & \text{for inelastic collision} \\ = 1 & \text{for perfectly elastic collision} \\ > 1 & \text{for superelastic collision} \end{cases} \tag{1.3}$$

The only case of elastic collision in Eq. 1.3 at the rebound time $t_1 = \tau$ in Eq. 1.2 preserves the kinetic energy. This hints us for construction of an energy restoring numerical scheme prescribing the rebound velocity as $v_1 = v_0$.

The paper is structured as follows. We formulate the collision problem for a bar moving with a high initial speed in the "Collision problem withhigh initial speed" section. The corresponding dynamic variational inequality is presented in a space-time rectangle for a wave equation subject to contact conditions over the obstacle. Its multiple solutions with discontinuous velocities are

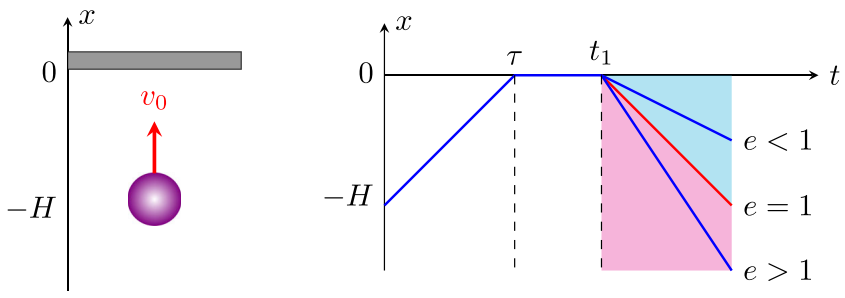

Fig. 1 Collision of a mass with an obstacle (left); multiple trajectories $x = u(t)$ (right)

constructed analytically in the "Multiple solutions with discontinuous velocities" section. The solutions are expressed by piecewise linear functions over suitable partitions of the rectangle, which do not coincide with characteristics of the wave equation. In the "ST-PDAS solution algorithm restoring energy" section, the problem is approximated by piecewise-linear functions on a uniform triangle grid. A particular numerical solution prescribed by the specific rebound velocity restoring the bar energy is presented in the "Numerical tests" section by the use of a ST-PDAS algorithm of SSN-type. Numerical tests of the collision benchmark demonstrate its high precision compared to the exact solution on grid points, super-linear convergence in very few iterates, and no oscillations of the discrete energy under grid refinement.

Collision problem with high initial speed

Let an isotropic linear elastic bar of the unit rigidity and density have the length $L > 0$. We assume that the bar is located below the origin at $x - L + u \in (-H - L, -H)$, with $H > 0$, in the reference configuration. Its motion starts when forced by an initial speed $v_0 > 0$ at time $t = 0$ without the gravity and initial deformation. See an illustration of the collision of the bar with an obstacle $x = 0$ in the left plot (a) of Fig. 2, which is drawn for $L = 1$, $H = 0.5$, and $v_0 = 2$.

For a final time $T > 0$ fixed, let us consider the time-space rectangle $Q = (0, T) \times (0, L)$ with the boundary ∂Q. We assume that the bar displacement $u(t, x)$ for ST-points $z := (t, x)$ is described by the wave equation with the unit propagation speed of elastic waves:

$$u_{,tt}(z) - u_{,xx}(z) = \lambda(z) \quad \text{for } z \in Q, \tag{2.1}$$

where λ is a contact force, which is expressed at the contact boundary by

$$\lambda(t, L) := u_{,x}(t, L) \quad \text{for } t \in (0, T). \tag{2.2}$$

Here, the first spatial derivative $u_{,x} = \partial u/\partial x$ corresponds to strain, and the second spatial derivative $u_{,xx} = \partial^2 u/\partial x^2$ is related to curvature. The lower bar end is free of stress at $x = 0$, that is:

$$\lambda(t, 0) := u_{,x}(t, 0) = 0 \quad \text{for } t \in (0, T), \tag{2.3}$$

whereas the upper bar end collides with the obstacle. To guarantee non-penetration of all bar points $x - L + u(t, x)$, $x \in [0, L]$, over the obstacle in all times $t > 0$, we impose the complementarity conditions:

$$\begin{cases} u(z) + x - L \le 0, \quad \lambda(z) \le 0, \quad \lambda(z)\big(u(z) + x - L\big) = 0 \\ \text{for } z = (t, x) \in \widetilde{Q} := \overline{Q} \setminus \{t = 0\}, \text{ where } \overline{Q} := Q \cup \partial Q. \end{cases} \tag{2.4}$$

The evolutionary equation is supported by the initial conditions at $t = 0$:

$$u(0, x) = -H, \quad u_{,t}(0, x) = v_0 \quad \text{for } x \in (0, L). \tag{2.5}$$

We give a variational formulation to the collision problem. By the Petrov–Galerkin method using the linear sub-spaces prescribed either by initial or final data [41]:

$$H^1_{0*}(0, T) := \{v \in H^1(0, T),\ v(0) = 0\}, \quad H^1_{*0}(0, T) := \{v \in H^1(0, T),\ v(T) = 0\},$$

we look for a weak solution in the trial space

$$V_{0*} = L^2(0, T; H^1(0, L)) \cap H^1_{0*}(0, T; L^2(0, L)),$$

which differs from the test space:

$$V_{*0} = L^2(0, T; H^1(0, L)) \cap H^1_{*0}(0, T; L^2(0, L)).$$

For smooth in $\overline{Q}$ functions u, v the Green formula holds:

$$\begin{aligned} &\int_Q (u_{,tt} - u_{,xx}) v \, dz = \int_Q (-u_{,t} v_{,t} + u_{,x} v_{,x}) \, dz \\ &+ \int_0^L u_{,t} v \, dx\big|_{t=0}^{T} - \int_0^T u_{,x} v \, dt\big|_{x=0}^{L}. \end{aligned} \tag{2.6}$$

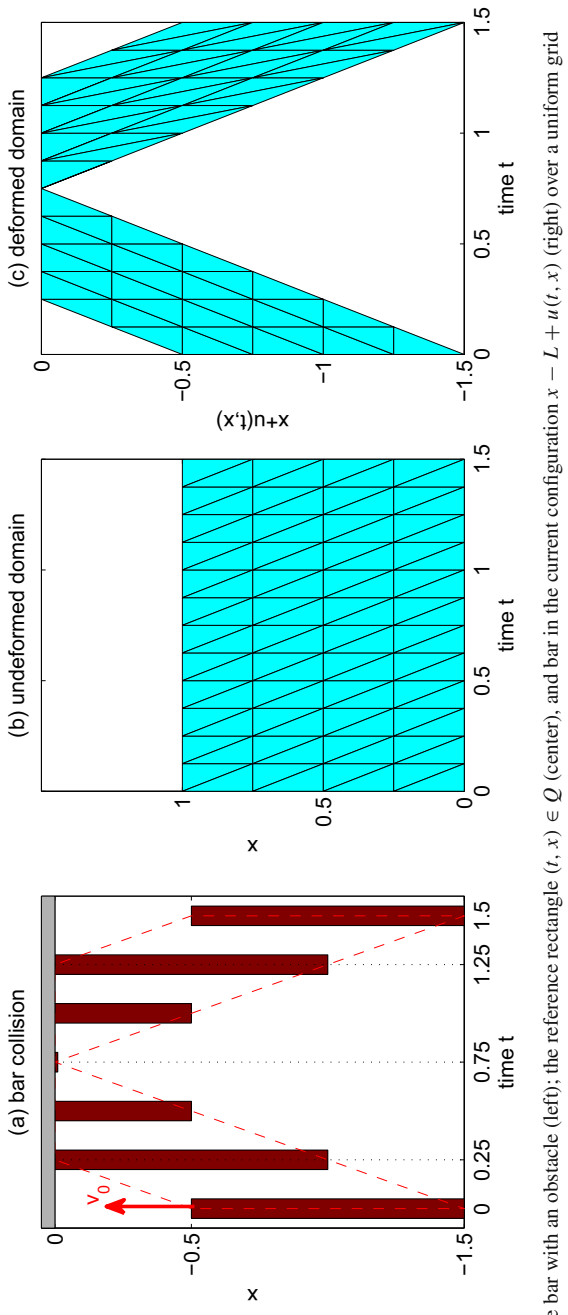

Fig. 2 Collision of the bar with an obstacle (left); the reference rectangle $(t, x) \in Q$ (center), and bar in the current configuration $x - L + u(t, x)$ (right) over a uniform grid

Inserting here relations (2.1)–(2.3) and (2.5), we get the equation:

$$\int_Q \lambda v\,dz = \int_Q (-u_{,t}v_{,t} + u_{,x}v_{,x})\,dz$$
$$+ \int_0^L u_{,t}v\,dx\big|_{t=T} - \int_0^L v_0 v\big|_{t=0}\,dx - \int_0^T \lambda v\,dt\big|_{x=L}.$$

Together with the complementarity conditions (2.4) this yields the primal-dual system for function pairs: Find $(u+H,\lambda) \in V_{0*} \times L^2(\widetilde{Q})$ such that

$$\begin{cases} u(z) + x - L \le 0, \quad \lambda(z) \le 0 \text{ for } z = (t,x) \in \widetilde{Q}, \\ \int_Q \lambda(u - L + x)\,dz + \int_0^T \lambda u\,dt\big|_{x=L} = 0, \\ \int_Q \lambda v\,dz + \int_0^T \lambda v\,dt\big|_{x=L} = \int_Q (-u_{,t}v_{,t} + u_{,x}v_{,x})\,dz - \int_0^L v_0 v\big|_{t=0}\,dx \end{cases} \tag{2.7}$$

for all test functions $v \in V_{*0}$. The smooth variational solution $u \in H^2(Q)$ to Eq. 2.7 guarantees that traces $u_{,x}$ exist at $x = 0, L$ and follows the point-wise relations (2.1)–(2.5) by converse arguments.

Using another representation following from Green's formula (2.6) tested with $v - u$ and accounting for relations (2.1)–(2.5):

$$\int_Q \lambda(v-u)\,dz = \int_Q \big(-u_{,t}(v_{,t} - u_{,t}) + u_{,x}(v_{,x} - u_{,x})\big)\,dz$$
$$+ \int_0^L u_{,t}(v-u)\,dx\big|_{t=T} - \int_0^L v_0(v\big|_{t=0} + H)\,dx - \int_0^T \lambda(v-u)\,dt\big|_{x=L}$$

by the virtue of decomposition $v - u = v + x - L - (u + x - L)$ reduces (2.7) to variational inequality: Find $u + H \in V_{0*}$ such that $u(z) + x - L \le 0$ for $z \in \widetilde{Q}$ and justifies

$$\begin{cases} 0 \le \int_Q \big(-u_{,t}(v_{,t} - u_{,t}) + u_{,x}(v_{,x} - u_{,x})\big)\,dz - \int_0^L v_0(v\big|_{t=0} + H)\,dx \\ \text{for all } v - u \in V_{*0} \text{ such that } v(z) + x - L \le 0 \text{ for } z = (t,x) \in \widetilde{Q}. \end{cases} \tag{2.8}$$

The contact force λ can be reconstructed in $\widetilde{Q}$ from solution u of the variational inequality (2.8) by solving the following equation:

$$\int_Q \lambda v\,dz + \int_0^T \lambda v\,dt\big|_{x=L} = \int_Q (-u_{,t}v_{,t} + u_{,x}v_{,x})\,dz - \int_0^L v_0 v\big|_{t=0}\,dx \tag{2.9}$$

for all test functions $v \in V_{*0}$.

Multiple solutions with discontinuous velocities

In the following, we construct solutions u to the variational inequality (2.8) and λ to Eq. 2.9, hence weak solutions (u,λ) to the boundary-value problem (2.1)–(2.5). The construction depends crucially on the initial speed $v_0 > 0$ in Eq. 2.5 compared to the propagation speed of elastic waves, which is taken 1 in the wave equation (2.1).

For moderate initial speeds $v_0 < 1$, a piece-wise linear solution to the variational inequality (2.8) was constructed early in the work [43]. The discontinuities take place across the characteristics $x - L = \tau - t$ and $x + L = t - \tau$ of the wave equation, where we recall the collision time $\tau = H/v_0$. The unique solution is given by the displacement $u(z)$ (left), velocity $u_t(z)$ (center), and strain $u_x(z)$ (right) depicted for $z \in \overline{Q}$ in the three plots of Fig. 3.

For high initial speeds $v_0 \ge 1$, we construct multiple piecewise-linear solutions to the variational inequality (2.8) as presented in the three plots (a), (b), and (c) of Fig. 4 corresponding to u, u_t, and u_x. The first discontinuity begins at the collision time $t = \tau$ across the line $(x - L)/v_0 = \tau - t$ that is prescribed uniquely by the initial speed. Whereas the second discontinuity is free across any line $x/v_1 + L/v_0 = t - \tau$ with an arbitrary speed $v_1 \ge 1$ starting from the rebound time $t = \tau + L/v_0$. These lines of discontinuity do not coincide with characteristics of the wave equation (2.1). Below, we prove this result rigorously.

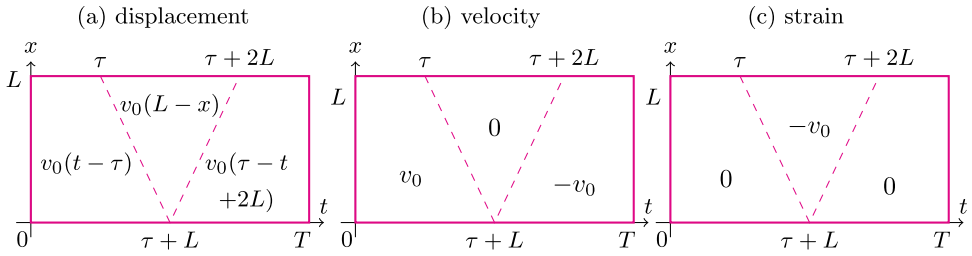

Fig. 3 Unique solution for $v_0 < 1$: displacement u (left); velocity u_t (center); strain u_x (right)

Theorem 1 *Let $T > \tau + L/v_0$. For the initial speed $v_0 \geq 1$ fixed, multiple solutions to the primal-dual variational problem (2.7) are given by*

$$u(z) = \begin{cases} v_0(t-\tau) & \text{in } K_1 := \left\{ z \in \overline{Q} : \ \frac{x-L}{v_0} \leq \tau - t \right\} \\ L - x & \text{in } K_2 := \left\{ z \in \overline{Q} : \ \frac{x-L}{v_0} \geq \tau - t, \ \frac{x}{v_1} + \frac{L}{v_0} \geq t - \tau \right\} \\ v_1(\tau - t + \frac{L}{v_0} + \frac{L}{v_1}) & \text{in } K_3 := \left\{ z \in \overline{Q} : \ \frac{x}{v_1} + \frac{L}{v_0} \leq t - \tau \right\} \end{cases} \tag{3.1}$$

with arbitrary $v_1 \geq 1$. The contact force in $\widetilde{Q}$ is represented by a discontinuous function:

$$\lambda(z) = \begin{cases} -1 & \text{for } z \in K_2 \cap \{x = L\} \\ \left(-v_0 + \frac{1}{v_0}\right)\left(1 + \frac{1}{v_0^2}\right)^{-1/2} & \text{for } z \in Q \cap \{\frac{x-L}{v_0} = \tau - t\} \\ \left(-v_1 + \frac{1}{v_1}\right)\left(1 + \frac{1}{v_1^2}\right)^{-1/2} & \text{for } z \in Q \cap \{\frac{x}{v_1} + \frac{L}{v_0} = t - \tau\} \\ 0 & \text{otherwise.} \end{cases} \tag{3.2}$$

Proof Let Γ_{12} be the interface between neighbor elements K_1 and K_2 with the normal vector $(1, 1/v_0)/\sqrt{1 + 1/v_0^2}$, and let Γ_{23} be the joint side between elements K_2 and K_3 with the normal vector $(1, -1/v_1)/\sqrt{1 + 1/v_1^2}$ in the partition K_1, K_2, K_3 of $\overline{Q}$. For short, we denote jumps of a field $w(z)$ over the interfaces by

$$[\![w]\!] = w\big|_{\partial K_2 \cap \Gamma_{12}} - w\big|_{\partial K_1 \cap \Gamma_{12}}, \quad [\![w]\!] = w\big|_{\partial K_3 \cap \Gamma_{23}} - w\big|_{\partial K_2 \cap \Gamma_{23}}.$$

The continuous, piece-wise linear function from Eq. 3.1 justifies equations:

$$\begin{cases} u_{,tt} = 0, \quad u_{,xx} = 0 & \text{in } K_1, K_2, K_3, \\ [\![u_{,t}]\!] = -v_0, \quad [\![u_{,x}]\!] = -1 & \text{on } \Gamma_{12} \\ [\![u_{,t}]\!] = -v_1, \quad [\![u_{,x}]\!] = 1 & \text{on } \Gamma_{23} \\ u\big|_{t=0} = -H, \quad u_{,t}\big|_{t=0} = v_0, \quad u_{,x}\big|_{x=0} = 0 & \text{on } \partial Q \\ u(t, L) = v_0(t - \tau), \quad u_{,x}(t, L) = 0 & \text{for } t \in [0, \tau] \\ u(t, L) = 0, \quad u_{,x}(t, L) = -1 & \text{for } t \in [\tau, \tau + \frac{L}{v_0} + \frac{L}{v_1}] \\ u(t, L) = v_1(\tau - t + \frac{L}{v_0} + \frac{L}{v_1}), \quad u_{,x}(t, L) = 0 & \text{for } t \in [\tau + \frac{L}{v_0} + \frac{L}{v_1}, T]. \end{cases} \tag{3.3}$$

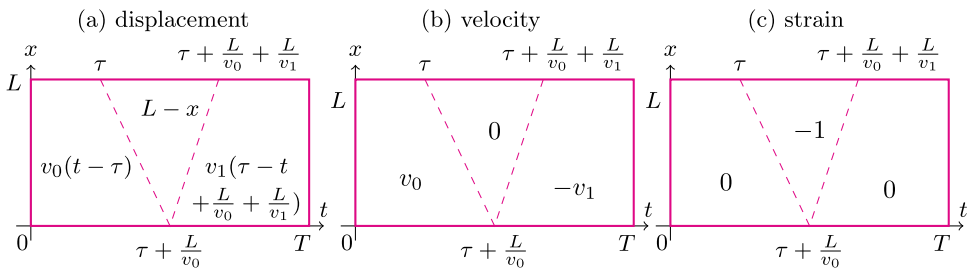

Fig. 4 Non-unique solutions for $v_0 \geq 1$: displacement u (left); velocity u_t (center); strain u_x (right)

From Green's formula (2.6) applied to piecewise-smooth functions u, v in K_1, K_2, K_3, which derivatives have jumps across Γ_{12} and Γ_{23}, we have the equation

$$\begin{aligned}\sum_{i=1}^{3}\int_{K_i}(u_{,tt}-u_{,xx})v\,dz &= \sum_{i=1}^{3}\int_{K_i}(-u_{,t}v_{,t}+u_{,x}v_{,x})\,dz\\ -\int_{\Gamma_{12}}\frac{[\![(u_{,t}-\frac{u_{,x}}{v_0})v]\!]}{\sqrt{1+\frac{1}{v_0^2}}}\,d\Gamma &- \int_{\Gamma_{23}}\frac{[\![(u_{,t}+\frac{u_{,x}}{v_1})v]\!]}{\sqrt{1+\frac{1}{v_1^2}}}\,d\Gamma + \int_0^L u_{,t}v\,dx\big|_{t=0}^{T} - \int_0^T u_{,x}v\,dt\big|_{x=0}^{L}.\end{aligned} \tag{3.4}$$

Let us insert (3.3) into (3.4) with smooth functions v such that $[\![v]\!]=0$. Using $[\![(u_{,t}-\frac{u_{,x}}{v_0})v]\!]=[\![u_{,t}-\frac{u_{,x}}{v_0}]\!]v$ on Γ_{12} and $[\![(u_{,t}+\frac{u_{,x}}{v_1})v]\!]=[\![u_{,t}+\frac{u_{,x}}{v_1}]\!]v$ on Γ_{23} yields

$$\begin{aligned}0 &= \int_Q(-u_{,t}v_{,t}+u_{,x}v_{,x})\,dz - \int_{\Gamma_{12}}\frac{-v_0+\frac{1}{v_0}}{\sqrt{1+\frac{1}{v_0^2}}}v\,d\Gamma - \int_{\Gamma_{23}}\frac{-v_1+\frac{1}{v_1}}{\sqrt{1+\frac{1}{v_1^2}}}v\,d\Gamma\\ &- \int_0^L v_0 v\big|_{t=0}\,dx + \int_\tau^{\tau+\frac{L}{v_0}+\frac{L}{v_1}} v\big|_{x=L}\,dt\end{aligned} \tag{3.5}$$

for all test functions $v\in V_{*0}$. By the virtue of formula (2.9), from Eq. 3.5, we determine the contact force in Eq. 3.2. The multiplier is non-positive for $v_0\geq 1$ and $v_1\geq 1$.

The gap between the obstacle and the displacement in Eq. 3.3 can be expressed on the partition as follows:

$$u(z)+x-L=\begin{cases}v_0\big(t-\tau+\frac{x-L}{v_0}\big) & \text{for } z\in K_1\\ 0 & \text{for } z\in K_2\\ v_1\big(\tau-t+\frac{L}{v_0}+\frac{x}{v_1}\big) & \text{for } z\in K_3,\end{cases} \tag{3.6}$$

hence the non-penetration condition $u+x-L\leq 0$ holds everywhere in $\widetilde{Q}$. From Eqs. 3.2 and 3.6, it follows the complementarity conditions in Eq. 2.7. The proof is completed. □

For the reason of thermodynamics, we introduce in the consideration a time-dependent function of the bar energy:

$$E(t):=\frac{1}{2}\int_0^L(u_{,t}^2+u_{,x}^2)\,dx,\quad t\in[0,T). \tag{3.7}$$

As a consequence of Theorem 1, we deduce the following.

Theorem 2 *If the assumptions of Theorem 1 hold, then the bar energy (3.7) is given by a continuous, piece-wise linear function such that*

$$E(t)=\begin{cases}\frac{1}{2}Lv_0^2 & \text{for } t\in[0,\tau)\\ \frac{1}{2}Lv_0^2-\frac{1}{2}v_0(v_0^2-1)(t-\tau) & \text{for } t\in[\tau,\tau+\frac{L}{v_0})\\ \frac{1}{2}L\big(1-\frac{v_1}{v_0}(v_1^2-1)\big)+\frac{1}{2}v_1(v_1^2-1)(t-\tau) & \text{for } t\in[\tau+\frac{L}{v_0},\tau+\frac{L}{v_0}+\frac{L}{v_1})\\ \frac{1}{2}Lv_1^2 & \text{for } t\in[\tau+\frac{L}{v_0}+\frac{L}{v_1},T).\end{cases} \tag{3.8}$$

Proof We calculate straightforwardly the bar energy (3.7) according to the solution formula (3.3). For $t\in[0,\tau)$, we have

$$2E(t)=\int_0^L v_0^2\,dx=Lv_0^2;$$

for $t\in[\tau,\tau+L/v_0)$:

$$2E(t)=\int_0^{L+v_0(\tau-t)}v_0^2\,dx+\int_{L+v_0(\tau-t)}^{L}(-1)^2\,dx=Lv_0^2-v_0(v_0^2-1)(t-\tau);$$

for $t\in[\tau+L/v_0,\tau+L/v_0+L/v_1)$:

$$\begin{aligned}2E(t) &= \int_0^{v_1(\tau-t)-Lv_1/v_0}(-v_1)^2\,dx+\int_{v_1(\tau-t)-Lv_1/v_0}^{L}(-1)^2\,dx\\ &= L\big(1-\frac{v_1}{v_0}(v_1^2-1)\big)+v_1(v_1^2-1)(t-\tau);\end{aligned}$$

and for $t \in [\tau + L/v_0 + L/v_1, T)$:

$$2E(t) = \int_0^L (-v_1)^2\, dx = Lv_1^2.$$

This completes the proof. □

We will use the analytical formulas obtained in Theorems 1 and 2 as a benchmark for the derivation of a numerical solution algorithm that restores the bar energy after rebound. It is based on the ST-FEM discretization of the collision problem on a uniform triangular grid and on the PDAS iteration of the complementarity conditions.

ST-PDAS solution algorithm restoring energy

We consider a partition $\cup_{i\in I} T_i = \overline{Q}$ of the space-time rectangle into equivalent elements given by right triangles T_i, $i \in I$. It composes a uniform triangulation with the temporal size $h_t = T/(N_t - 1)$ in t-direction, and the spatial size $h_x = L/(N_x - 1)$ in x-direction, where integers $N_t, N_x \geq 2$. Moreover, we assume the relation $h_t = h_x/v_0$ according to the initial speed. The grid has the number $N_t N_x$ of nodes in $\overline{Q}$ corresponding to degrees of freedom DOF, and a number $M = (N_t - 1)N_x$ of constrained nodal points in $\widetilde{Q}$. An example grid for $N_x = 5$ and $N_t = 13$ is illustrated in the center plot (b) of Fig. 2. We set the vector-valued mesh-size parameter $h = (h_t, h_x)$.

On this partition, a full ST-discretization will be implemented in the standard space of continuous, piece-wise linear functions for displacements:

$$V^h = \big\{v_h \in C(\overline{Q}), \quad v_h\big|_{T_i} \in \mathbb{P}_1(T_i) \text{ for } i \in I\big\}.$$

The trial V_{0*} and test V_{*0} spaces are approximated by respective finite-element spaces:

$$V_{0*}^h = \big\{v_h \in V^h,\ v_h(0,\,\cdot\,) = 0\big\}, \quad V_{*0}^h = \big\{v_h \in V^h,\ v_h(T,\,\cdot\,) = 0\big\}.$$

We associate ST-nodal points $z_h := (t_h, x_h) \in \overline{Q}$ with usual hat-type functions ϕ_h building a nodal basis of the dimension DOF in V^h. For the contact force, we will use a piece-wise constant $\mathbb{P}_0$-approximation. To fit the discontinuous function λ in the analytical formula (3.2), this leads to a nodal representation by the Lagrange multiplier λ_h in M constrained nodes over $\widetilde{Q}$. Then, we approximate the primal-dual system (2.7): Find $(u_h + H, \lambda_h) \in V_{0*}^h \times \mathbb{R}^M$ such that

$$\begin{cases} u_h(z_h) + x_h - L \leq 0, \quad \lambda_h \leq 0, \quad \lambda_h\big(u_h(z_h) + x_h - L\big) = 0 \text{ for } z_h \in \widetilde{Q}, \\ \lambda_h = \displaystyle\int_Q (-u_{h,t}\phi_{h,t} + u_{h,x}\phi_{h,x})\, dz - \int_0^L v_0\phi_h\big|_{t=0}\, dx \end{cases} \tag{4.1}$$

for all basis functions $\phi_h \in V_{*0}^h$.

For $r > 0$ fixed, let us define complementary, primal-dual active $\mathcal{A}$ and inactive $\mathcal{I}$ sets splitting the constrained nodes:

$$\begin{cases} \mathcal{A}(u_h, \lambda_h) = \big\{z_h \in \widetilde{Q} :\ r\lambda_h - u_h(z_h) - x_h + L < 0\big\} \\ \mathcal{I}(u_h, \lambda_h) = \big\{z_h \in \widetilde{Q} :\ r\lambda_h - u_h(z_h) - x_h + L \geq 0\big\}. \end{cases} \tag{4.2}$$

As a consequence of the complementarity conditions in Eq. 4.1, two options follow:

$$\begin{cases} u_h(z_h) + x_h - L = 0, \quad \lambda_h < 0 \quad \text{on } \mathcal{A}(u_h, \lambda_h) \\ u_h(z_h) + x_h - L \leq 0, \quad \lambda_h = 0 \quad \text{on } \mathcal{I}(u_h, \lambda_h). \end{cases} \tag{4.3}$$

With the help of Eqs. 4.2 and 4.3, problem (4.1) is equivalent to an implicit variational equation on a linear subspace: Find $u_h + H \in V_{0*}^h$ such that

$$\begin{cases} u_h(z_h) + x_h - L = 0 \text{ on } \mathcal{A}(u_h, \lambda_h), \\ \displaystyle\int_Q (-u_{h,t}\phi_{h,t} + u_{h,x}\phi_{h,x})\, dz - \int_0^L v_0\phi_h\big|_{t=0}\, dx = 0 \\ \text{for all } \phi_h \in V_{*0}^h \text{ with } \phi_h = 0 \text{ on } \mathcal{A}(u_h, \lambda_h), \end{cases} \tag{4.4}$$

and $\lambda_h \in \mathbb{R}^M$ such that

$$\lambda_h = \begin{cases} r_h & \text{on } \mathcal{A}(u_h, \lambda_h) \\ 0 & \text{on } \mathcal{I}(u_h, \lambda_h), \end{cases} \tag{4.5}$$

where the residual $r_h \in \mathbb{R}^{\mathrm{DOF}}$:

$$r_h = \int_Q (-u_{h,t}\phi_{h,t} + u_{h,x}\phi_{h,x})\,dz - \int_0^L v_0\phi_h\big|_{t=0}\,dx \tag{4.6}$$

for all basis functions $\phi_h \in V^h_{*0}$.

Following [29, 30], we iterate the equations (4.2), (4.4)–(4.6) over the primal-dual active sets in the following algorithm.

Algorithm 1 ST-PDAS

1: Initialize active set $\mathcal{A}^0 = \emptyset$ and set iteration number $k = 0$.

2: Solve the linear system with respect to $u^k_h + H \in V^h_{0*}$:

$$\begin{cases} u^k_h(z_h) + x_h - L = 0 \text{ on } \mathcal{A}^k_h, \\ \displaystyle\int_Q (-u^k_{h,t}\phi_{h,t} + u^k_{h,x}\phi_{h,x})\,dz - \int_0^L v_0\phi_h\big|_{t=0}\,dx = 0 \\ \text{for all } \phi_h \in V^h_{*0} \text{ with } \phi_h = 0 \text{ on } \mathcal{A}^k_h. \end{cases} \tag{4.7}$$

3: Compute the residual $r^k_h \in \mathbb{R}^{\mathrm{DOF}}$:

$$r^k_h = \int_Q (-u^k_{h,t}\phi_{h,t} + u^k_{h,x}\phi_{h,x})\,dz - \int_0^L v_0\phi_h\big|_{t=0}\,dx \text{ for all } \phi_h \in V^h_{*0}. \tag{4.8}$$

4: Compute the Lagrange multiplier $\lambda^k_h \in \mathbb{R}^M$:

$$\lambda^k_h = \begin{cases} r^k_h & \text{on } \mathcal{A}^k_h \\ 0 & \text{on } \mathcal{I}^k_h. \end{cases} \tag{4.9}$$

5: Update the primal-dual active and inactive sets:

$$\begin{cases} \mathcal{A}^{k+1}_h = \{z_h \in \widetilde{Q} :\ r\lambda^k_h - u^k_h(z_h) - \delta_1 - (1-\delta_2)(x_h - L) < 0\} \\ \mathcal{I}^{k+1}_h = \{z_h \in \widetilde{Q} :\ r\lambda^k_h - u^k_h(z_h) - \delta_1 - (1-\delta_2)(x_h - L) \geq 0\}. \end{cases} \tag{4.10}$$

6: Terminate iteration if it cycles, or the termination condition holds:

$$\mathcal{A}^{k+1}_h = \mathcal{A}^k_h, \tag{4.11}$$

otherwise increase iteration number $k = k + 1$ and go to step 2.

The discrete problem (4.1) may obey multiple solutions as well as the continuous problem (2.7). In this case, basic iterations **1:–6:** would cycle or diverge. Therefore, we specify the ST-PDAS algorithm in such a way to get a unique solution corresponding to the restitution coefficient $e = 1$ in Eq. 1.3. It is thermodynamically reasonable since the velocity $v_1 = v_0$ restores the energy E after rebound according to the analytical formula (3.8). The below heuristics were helpful in our numerical tests for stable convergence of the ST-PDAS algorithm without cycling.

7: Small parameters δ_1 and δ_2 in Eq. 4.10 regularize grazing contact in Q. There are taken $\delta_1 = \delta_2 = 10^{-10}$, and $r = 10^{-2}$.

8: We extend the final time to match the trial V^h_{0*} and the test V^h_{*0} spaces by widening Q to the computational domain $(0, T + 2h_t) \times (0, L)$.

9: At the contact interface $\{x = L\}$, we say that collision starts at a node where $(t^k_h - h_t, L) \in \mathcal{I}^k_h$ and $(t^k_h, L) \in \mathcal{A}^k_h$ (that corresponds to τ for the analytical solution). Just before the collision and for the extended times, the stress-free condition $u^k_{h,x}(t_h, L) = 0$ in Eq. 3.3 is realized by the finite difference:

$$u^k_h(t_h, L) - u^k_h(t_h, L - h_x) = 0 \quad \text{for } t_h \in \{t^k_h - h_t, T + h_t, T + 2h_t\}. \tag{4.12}$$

10: In $\widetilde{Q} \setminus \{x = L\}$, collision starts at a set Γ^k_{12h} where $(t^k_h - h_t, x^k_h) \in \mathcal{I}^k_h$ and $z^k_h := (t^k_h, x^k_h) \in \mathcal{A}^k_h$ (corresponding to Γ_{12} in Eq. 3.3). Therefore, just after the collision, we impose zero velocity $u^k_{h,t}(z^k_h) = 0$ using the finite difference:

$$u^k_h(t^k_h + h_t, x^k_h) - u^k_h(t^k_h, x^k_h) = 0 \quad \text{for } z^k_h \in \Gamma^k_{12h}. \tag{4.13}$$

11: In $\widetilde{Q} \setminus \{x = L\}$, the bar rebounds at a set Γ^k_{23h} where $z^k_h := (t^k_h, x^k_h) \in \mathcal{A}^k_h$ and $(t^k_h + h_t, x^k_h) \in \mathcal{I}^k_h$ (corresponding to Γ_{23} in Eq. 3.3). Following the restitution $e = 1$, we impose the velocity $u^k_{h,t}(z^k_h) = -v_0$, which is expressed by the finite difference:

$$u^k_h(t^k_h + h_t, x^k_h) - u^k_h(t^k_h, x^k_h) = -h_t \quad \text{for } z^k_h \in \Gamma^k_{23h}. \tag{4.14}$$

12: In the case of intersection $z^k_h := (t^k_h, x^k_h) \in \Gamma^k_{23h} \cap \Gamma^k_{23h}$, we have $v_1 = v_0$. In this node, Eqs. 4.13 and 4.14 should be replaced with the finite difference:

$$-u^k_h(t^k_h - h_t, x^k_h) + 2u^k_h(t^k_h, x^k_h) - u^k_h(t^k_h + h_t, x^k_h) = 2h_t. \tag{4.15}$$

13: To preserve a monotone decrease of active sets over rebound time for $k \geq 1$, we re-initialize (4.10) if repeated active sets increase:

$$\mathcal{A}^{k+1}_h := \mathcal{A}^{k+1}_h \setminus \{z_h \in \Gamma^{k+1}_{23h} \text{ such that } z_h \in \mathcal{A}^{k+1}_h \cap \mathcal{A}^k_h \text{ but } z_h \notin \mathcal{A}^k_h \cap \mathcal{A}^{k-1}_h\}. \tag{4.16}$$

14: Implementing conditions **10:–13:** over the set $\widetilde{Q} \setminus \{x = L\}$, this needs to relax the Dirichlet condition stated in Eq. 4.7 on $\mathcal{A}^k_h$ to the contact boundary $\mathcal{A}^k_h \cap \{x = L\}$.

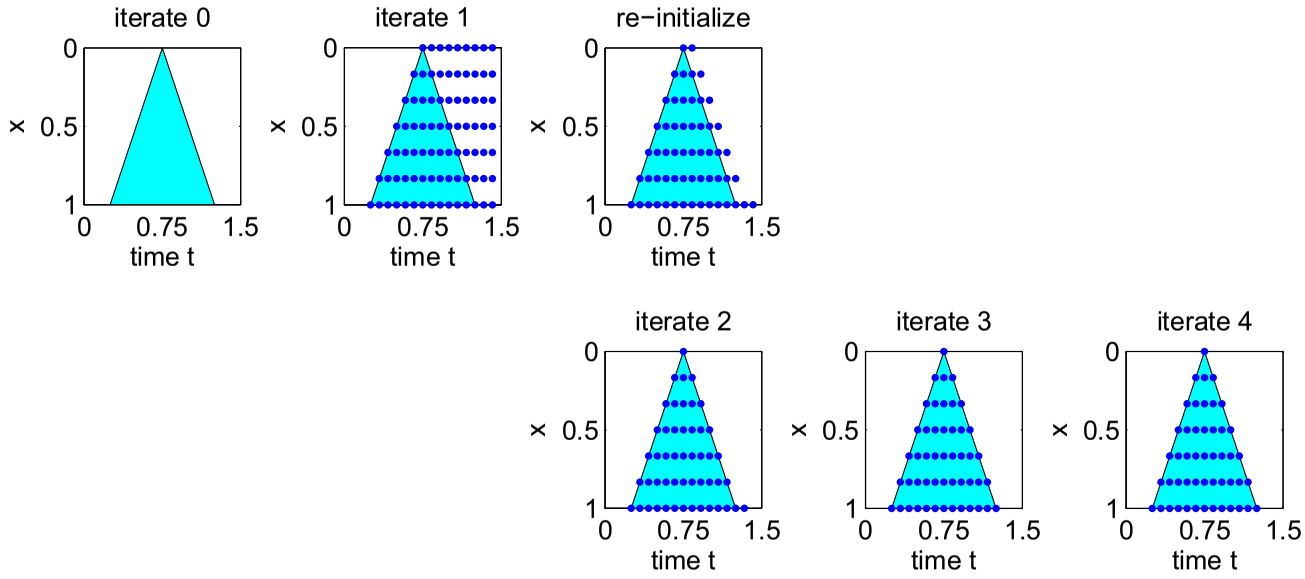

Fig. 5 ST-PDAS iterates of active sets $\mathcal{A}_h^0, \ldots, \mathcal{A}_h^3 = \mathcal{A}_h^4$ in $Q = (0, 1.5) \times (0, 1)$, $v_0 = 2$ as $N_x = 7$

Table 1 Discretization parameters corresponding to the number N_x

N_x	h_x	N_t	h_t	DOF	M
5	0.25	13	0.125	65	60
7	0.16..	19	0.083..	133	126
9	0.125	25	0.0625	225	216
11	0.1	31	0.05	341	330
21	0.05	61	0.025	1281	1260
31	0.03..	91	0.016..	2821	2790
41	0.025	121	0.0125	4961	4950
51	0.02	151	0.01	7701	7650

See the example of re-initialization at $k = 2$ in Fig. 5 presenting the numerical solution in $\overline{Q} = [0, 1.5] \times [0, 1]$. The problem is discretized by the numbers $N_x = 7$, and $N_t = 19$ as the initial speed $v_0 = 2$, thus DOF= 133 with $M = 126$ constrained nodes in $\widetilde{Q} = (0, 1.5] \times [0, 1]$. The figure shows history of active points during the iterates $k = 0, \ldots, 4$ along with the filled triangle presenting the true active set $\{(x-1)/2 \geq 1/2-t, (x+1)/2 \geq t-1/4\}$ for which the exact solution satisfies $r\lambda - u - x + L < 0$.

In the next section, we validate in details the ST-PDAS algorithm implemented between the lines **1:–14:** for the collision benchmark given in Theorem 1.

Numerical tests

In further numerical tests, we set the bar length $L = 1$ and final time $T = 1.5$ such that the reference rectangle $Q = (0, 1.5) \times (0, 1)$, the initial depth $H = 0.5$ and initial speed $v_0 = 2$ with the collision time $\tau = 2$, portrayed in Fig. 2.

Further discretization numbers N_x in x-direction are varied in the range of $5, \ldots, 51$. The values $N_t = 3(N_x - 1) + 1$ corresponding to t-direction are provided by $v_0 = 2$. The numbers of DOF and constraints M are gathered in Table 1 along with the mesh sizes h_t and h_x.

Table 2 collects the number of iterations #it that are required for termination of the ST-PDAS algorithm and presented versus discretization numbers. It clearly demonstrates that the growth of #it is very moderate under increasing N_x.

For $N_x = 7$, the history of displacement iterates $u_h^0, \ldots, u_h^3$ is depicted in Fig. 6. Iterates of the Lagrange multiplier $\lambda_h^0, \ldots, \lambda_h^3$ are portrayed in Fig. 7.

We compare discrete displacements u_h with the exact solution u along the contact boundary $x = 1$. Figure 8 presents the result of comparison by varying step-sizes h_t selected in the range of $0.01, \ldots, 0.05$. In the left plot (a), the functions $u_h(t, 1)$ and $u(t, 1)$ are depicted with respect to time $t \in (0, 1.5)$, and they all are visually indistinguishable. The right plot (b) shows the maximum error:

$$\max_{t\in(0,1.5)} |u_h(t, 1) - u(t, 1)|$$

versus h_t, which is less that 10^{-13} for all step-sizes.

Finally, we calculate the exact energy E of the bar given by formula (3.8) with $L = 1$, $v_1 = v_0 = 2$, $\tau = 1/4$ and $L/v_1 = L/v_0 = 1/2$ such that

$$E(t) = \begin{cases} 2 & \text{for } t \in [0, 0.25) \\ 2 - 3(t - 0.25) & \text{for } t \in [0.25, 0.75) \\ 3(t - 0.25) - 1 & \text{for } t \in [0.75, 1.25) \\ 2 & \text{for } t \in [1.25, 1.5). \end{cases}$$

The discrete energy E_h is computed in equidistant time points $t^1, \ldots, t^{N_t}$ according to the formula (3.7) and compared with the exact values $E(t^m)$, for $m = 1, \ldots, N_t$.

Table 2 Number of iterations #it required to terminate ST-PDAS algorithm

N_x	5	7	9	11	21	31	41	51
#it	3	4	5	5	6	5	7	7

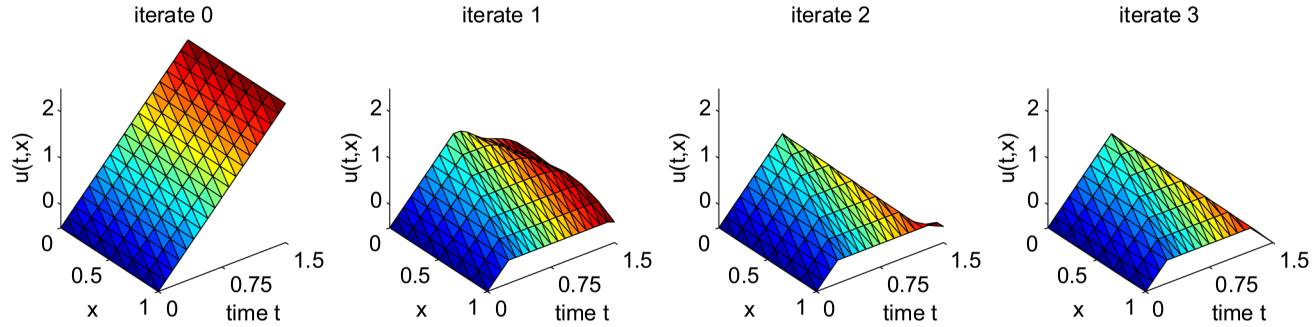

Fig. 6 ST-PDAS iterates $k = 0, \ldots, 3$ of the displacement u_h^k as $N_x = 7$

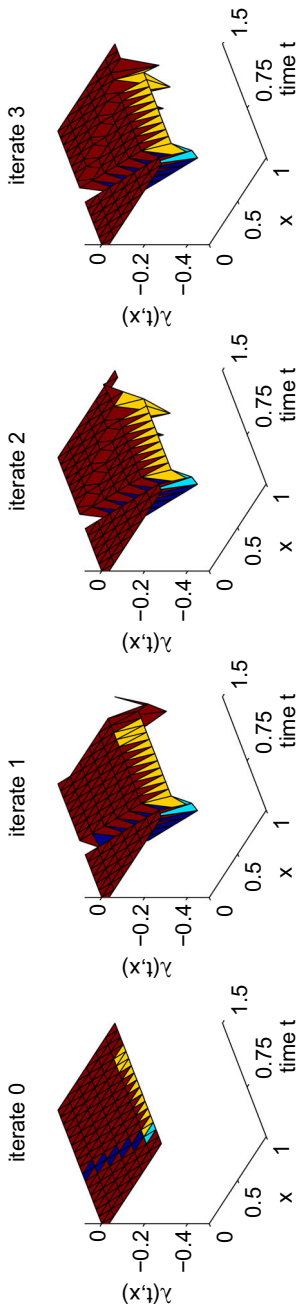

Fig. 7 ST-PDAS iterates $k = 0, \ldots, 3$ of the Lagrange multiplier λ_h^k as $N_x = 7$

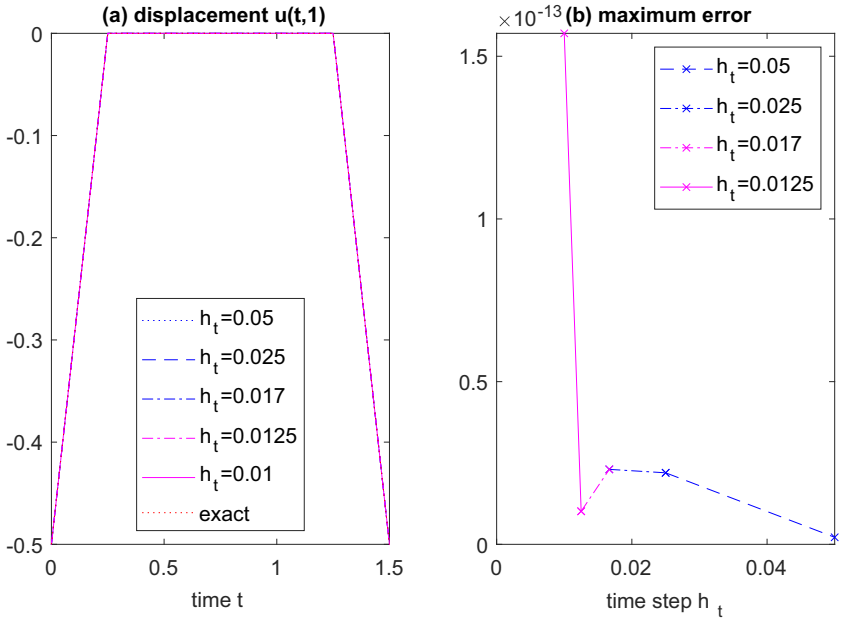

Fig. 8 Discrete displacements $u_h(t, 1)$ for step-sizes h_t compared with the exact solution $u(t, 1)$ at the contact boundary

The left plot (a) of Fig. 9 depicts the curves $E_h(t)$ and $E(t)$ versus time $t \in (0, 1.5)$. In the figure, we observe that discrete energies coincide before rebound $t < 0.75$, and they approach the exact energy after the rebound $t \geq 0.75$. In the right plot (b) of Fig. 9 the relative error with respect to the discrete L^2-norm:

$$\sqrt{h_t \sum_{m=1}^{N_t} \left(\frac{E_m - E(t^m)}{E(t^m)}\right)^2} \times 100\ (\%)$$

is drawn versus the step-size h_t. This curve has a slightly increasing slope when h_t drops, thus a super-linear convergence rate.

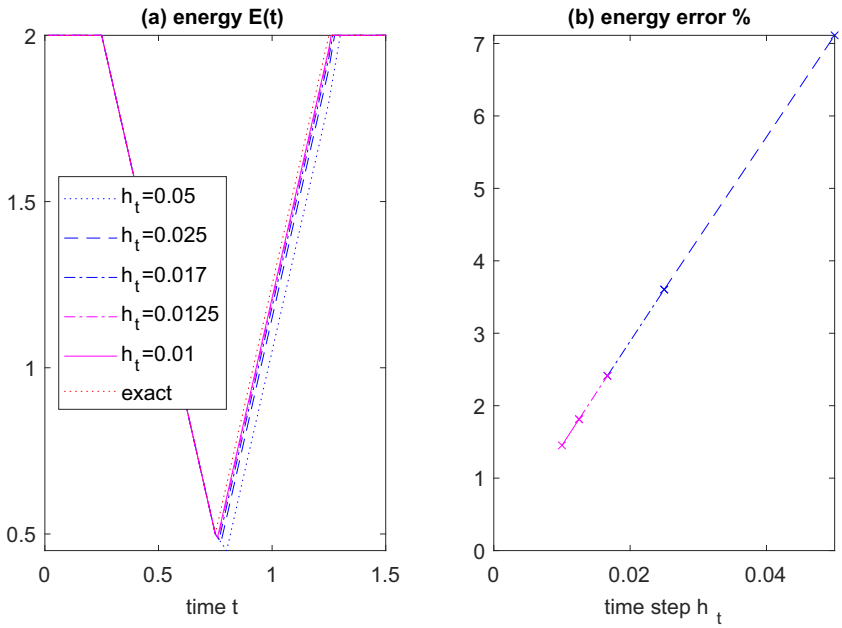

Fig. 9 Discrete energies $E_h(t)$ for step-sizes h_t compared with the exact energy $E(t)$

Conclusions

To treat collision problems with a discontinuous velocity, we elaborate a space-time finite-element method and endow it with a primal-dual active set algorithm. The ST-PDAS algorithm in two space-time dimensions is applied to an analytical benchmark of a rigid obstacle collided by an elastic bar with a high initial speed v_0 which exceeds the propagation speed of elastic waves equals 1 here. We select a unique solution following the restitution coefficient $e = 1$ that restores the energy of the bar after rebound. We present numerical tests on a uniform triangulation of the space-time domain. When supported by a re-initialization procedure, the ST-PDAS iterates converge in 3–7 iterates for all discretizations tested. The numerical solution on nodes coincides with the exact solution even for coarse grids. The energy converges with a super-linear rate under grid refinement without spurious oscillations. For the advantages of the ST-PDAS approach over with time-stepping methods, see the recent work [44]. Accounting for the gravity may be the subject for a future research.

Acknowledgements The author acknowledges the financial support by the University of Graz. He thanks the Georgian Mathematical Union for the long-time collaboration.

Author contribution Conceptualization: V.A.K.

Funding Open access funding provided by University of Graz.

Data availibility Data is contained within the article and available from the corresponding author on reasonable request.

Declarations

Conflict of interest The author declares no competing interests.

Open Access This article is licensed under a Creative Commons Attribution 4.0 International License, which permits use, sharing, adaptation, distribution and reproduction in any medium or format, as long as you give appropriate credit to the original author(s) and the source, provide a link to the Creative Commons licence, and indicate if changes were made. The images or other third party material in this article are included in the article's Creative Commons licence, unless indicated otherwise in a credit line to the material. If material is not included in the article's Creative Commons licence and your intended use is not permitted by statutory regulation or exceeds the permitted use, you will need to obtain permission directly from the copyright holder. To view a copy of this licence, visit http://creativecommons.org/licenses/by/4.0/.

References

1. Laursen, T.A.: Computational Contact and Impact Mechanics. Springer, Berlin, Heidelberg (2003). https://doi.org/10.1007/978-3-662-04864-1
2. Wriggers, P.: Computational Contact Mechanics. Springer, Berlin, Heidelberg (2006). https://doi.org/10.1007/978-3-540-32609-0
3. Vekua, N.P.: Systems of Singular Integral Equations. P. Noordhoff, University of Michigan (1967)
4. Buchukuri, T., Chkadua, O., Duduchava, R.: Crack-type boundary value problems of electro-elasticity. In: Gohberg, I., Wendland, W., Ferreira-dos-Santos, A., Speck, F.-O., Sepúlveda-Teixeira, F. (eds.) Operator Theoretical Methods and Applications to Mathematical Physics vol. 147, pp. 189–212. Birkhüuser, Basel (2004). https://doi.org/10.1007/978-3-0348-7926-2_26
5. Gachechiladze, A., Gachechiladze, R., Natroshvili, D.: Dynamical contact problems with friction for hemitropic elastic solids. Georgian Math. J. **21**(2), 165–185 (2009) https://doi.org/10.1515/gmj-2014-0024
6. Popov, V.G.: A dynamic contact problem which reduces to a singular integral equation with two fixed singularities. J. Appl. Math. Mech. **76**(3), 348–357 (2012) https://doi.org/10.1016/j.jappmathmech.2012.07.012
7. Khludnev, A.M., Kovtunenko, V.A.: Analysis of Cracks in Solids. Int. Ser. Adv. Fract. Mech., vol. 6. WIT-Press, Southampton, Boston (2000)
8. Bach, M., Kovtunenko, V.A., Khludnev, A.M.: Derivatives of the energy functional for 2D-problems with a crack under Signorini and friction conditions. Math. Meth. Appl. Sci. **23**(6), 515–534 (2000) https://doi.org/10.1002/(SICI)1099-1476(200004)23:6<515::AID-MMA122>3.0.CO;2-S
9. Cakoni, F., Kovtunenko, V.A.: Topological optimality condition for the identification of the center of an inhomogeneity. Inverse Probl. **34**(3), 035009 (2018) https://doi.org/10.1088/1361-6420/aaa997
10. Khludnev, A.M., Kovtunenko, V.A., Tani, A.: On the topological derivative due to kink of a crack with non-penetration. anti-plane model. J. Math. Pures Appl. **94**(6), 1219–1253 (2010) https://doi.org/10.2969/jmsj/06041219
11. Popova, T.S.: On orthogonal junction of thin semi-rigid inclusions in a two-dimensional elastic body. Comput. Math. Model. **36**(1), 126–138 (2025) https://doi.org/10.1007/s10598-025-09627-x
12. Argatov, I., Papangelo, A.: Adhesive contact of a viscoelastic fibrillar surface — a homogenized model. Mech. Res. Commun. **149**, 104535 (2025) https://doi.org/10.1016/j.mechrescom.2025.104535
13. Itou, H., Kovtunenko, V.A., Rajagopal, K.R.: Crack problem within the context of implicitly constituted quasi-linear viscoelasticity. Math. Mod. Meth. Appl. Sci. **29**(2), 355–372 (2019) https://doi.org/10.1142/S0218202519500118
14. Itou, H., Kovtunenko, V.A., Rajagopal, K.R.: Nonlinear model of a porous body with fluid-driven fracture under cohesion contact conditions and fluid volume control. Math. Mod. Meth. Appl. Sci. **35**(11), 2311–2328 (2025) https://doi.org/10.1142/S021820252550040X
15. Han, W., Migórski, S., Sofonea, M.: Analysis of a general dynamic history-dependent variational–hemivariational inequality. Nonlinear Anal. Real World Appl. **36**, 69–88 (2017) https://doi.org/10.1016/j.nonrwa.2016.12.007

16. Kashiwabara, T., Itou, H.: Unique solvability of a crack problem with Signorini-type and Tresca friction conditions in a linearized elastodynamic body. Phil. Trans. R. Soc. A. **380**(2236), 20220225 (2022) https://doi.org/10.1098/rsta.2022.0225
17. Gou, K., Mallikarjunaiah, S.M.: Finite element study of V-shaped crack-tip fields in a three-dimensional nonlinear strain-limiting elastic body. Math. Meth. Solids. **28**(10), 2155–2176 (2023) https://doi.org/10.1177/10812865221152257
18. Nikiforov, D.Y., Stepanov, S.P., Lazarev, N.P.: Online meshfree generalized multiscale finite element method for flows in fractured media. Lobachevskii J. Math. **45**(11), 5391–5401 (2024) https://doi.org/10.1134/S1995080224606647
19. Furtsev, A.I., Rudoy, E.M., Sazhenkov, S.A.: On hyperelastic solid with thin rigid inclusion and crack subjected to global injectivity condition. Phil. Trans. R. Soc. A. **382**(2277), 20240115 (2024) https://doi.org/10.1098/rsta.2024.0115
20. Gwinner, J., Jadamba, B., Khan, A.A., Raciti, F.: Uncertainty Quantification in Variational Inequalities: Theory, Numerics, and Applications. Chapman and Hall/CRC, New York (2021). https://doi.org/10.1201/9781315228969
21. Nápoles, G., Salmeron, J.L., Salgueiro, Y.: Inverse simulation learning of quasi-nonlinear fuzzy cognitive maps. Neurocomputing. **650**, 130864 (2025) https://doi.org/10.1016/j.neucom.2025.130864
22. Rudoy, E.M., Sazhenkov, S.A.: The homogenized dynamical model of a thermoelastic composite stitched with reinforcing filaments. Phil. Trans. R. Soc. A. **382**(2277), 20230304 (2024) https://doi.org/10.1098/rsta.2023.0304
23. Alekseev, G.V., Spivak, Y.E.: Correctness analysis of a boundary value problem for stationary magnetohydrodynamics equations with variable coefficients. Diff. Equat. **61**(4), 452–469 (2025) https://doi.org/10.1134/S0012266125040044
24. Chok, J., Petzinna, D.: Constrained Dikin–Langevin diffusion for polyhedra. arXiv:2510.04582. (2025) https://doi.org/10.48550/arXiv.2510.04582
25. Efendiev, M., Vougalter, V.: On the well-posedness of some model arising in the mathematical biology. Math. Meth. Appl. Sci. **48**(3), 3670–3681 (2025) https://doi.org/10.1002/mma.10507
26. Li, W., Sun, J., Pang, Y.: Periodic solutions for a class of 2n-order ordinary differential equations. Mathematics. **13**(17), 2757 (2025) https://doi.org/10.3390/math13172757
27. Chouly, F., Hild, P., Renard, Y.: Finite Element Approximation of Contact and Friction in Elasticity. Birkhäuser, Cham (2023). https://doi.org/10.1007/978-3-031-31423-0
28. Ito, K., Kunisch, K.: Lagrange Multiplier Approach to Variational Problems and Applications. SIAM, Philadelphia, PA (2008). https://doi.org/10.1137/1.9780898718614
29. Hintermüller, M., Kovtunenko, V.A., Kunisch, K.: Generalized Newton methods for crack problems with non-penetration condition. Numer. Meth. Partial Differ. Equ. **21**(3), 586–610 (2005) https://doi.org/10.1002/num.20053
30. Hintermüller, M., Kovtunenko, V.A., Kunisch, K.: A Papkovich–Neuber-based numerical approach to cracks with contact in 3D. IMA J. Appl. Math. **74**(3), 325–343 (2009) https://doi.org/10.1093/imamat/hxp017
31. Hager, C., Hauret, P., Le-Tallec, P., Wohlmuth, B.I.: Solving dynamic contact problems with local refinement in space and time. Comput. Meth. Appl. Mech. Eng. **201–204**(2), 25–41 (2012) https://doi.org/10.1016/j.cma.2011.09.006
32. Zhang, Z., Barboteu, M., Cao, J.: A class of time-dependent variational inequalities and their application in multi-layer contact systems. Nonlinear Anal. Real World Appl. **85**, 104338 (2025) https://doi.org/10.1016/j.nonrwa.2025.104338
33. Kovtunenko, V.A., Renard, Y.: FEM approximation of dynamic contact problem for fracture under fluid volume control using HHT-α and semi-smooth Newton methods. Appl. Numer. Math. **218**, 148–158 (2025) https://doi.org/10.1016/j.apnum.2025.07.009
34. Kovtunenko, V.A., Renard, Y.: Convergence analysis of semi-smooth Newton method for mixed FEM approximations of dynamic two-body contact and crack problems. J. Comput. Appl. Math. **471**, 116722 (2026) https://doi.org/10.1016/j.cam.2025.116722
35. Dirani, N., Monasse, L.: An explicit pseudo-energy conservative scheme for contact between deformable solids. Int. J. Numer. Meth. Engng. **125**(4), 7395 (2024) https://doi.org/10.1002/nme.7395
36. Doyen, D., Ern, A., Piperno, S.: Time-integration schemes for the finite element dynamic Signorini problem. SIAM J. Sci. Comput. **33**(1), 223–249 (2011) https://doi.org/10.1137/100791440
37. Dabaghi, F., Krejčí, P., Petrov, A., Pousin, J., Renard, Y.: A weighted finite element mass redistribution method for dynamic contact problems. J. Comput. Appl. Math. **345**(8), 338–356 (2019) https://doi.org/10.1016/j.cam.2018.06.030
38. Dabaghi, F., Petrov, A., Pousin, J., Renard, Y.: A robust finite element redistribution approach for elastodynamic contact problems. Appl. Numer. Math. **103**, 48–71 (2016) https://doi.org/10.1016/j.apnum.2015.12.004
39. Khenous, H.B., Laborde, P., Renard, Y.: Comparison of two approaches for the discretization of elastodynamic contact problems. C. R. Acad. Sci. Paris Ser. I. **342**(10), 791–796 (2006) https://doi.org/10.1016/j.crma.2006.03.011
40. Langer, U., Steinbach, O. (eds.): Space-Time Methods: Applications to Partial Differential Equations. De Gruyter, Berlin (2019)
41. Zank, M.: Efficient direct space-time finite element solvers for the wave equation in second-order formulation. J. Sci. Comput. **105**(1), 19 (2025) https://doi.org/10.1007/s10915-025-03038-1
42. Kovtunenko, V.A.: Space-time finite element based primal-dual active set method for the non-smooth problem of impact of rigid obstacle by elastic bar. Comput. Math. Model. **36**(1), 571–596 (2025) https://doi.org/10.1016/j.matpur.2010.06.002
43. Kovtunenko, V.A.: Space-time primal-dual active set method: benchmark for collision of elastic bar with discontinuous velocity. Computation. **13**(9), 210 (2025) https://doi.org/10.3390/computation13090210
44. Kovtunenko, V.A., Petrov, A., Renard, Y.: Space-time FEM solution of dynamic contact problem with discontinuous velocity for multiple impact of deformed bar using PDAS method. Math. Meth. Appl. Sci. (2025) https://doi.org/10.1002/mma.70370

Publisher's Note Springer Nature remains neutral with regard to jurisdictional claims in published maps and institutional affiliations.